Automatic segmentation of MR images for long-bone cross-sectional image analysis

S. Lam[1], H. Salilgheh Rad[1], J. Magland[1], and F. W. Wehrli[1]
[1]Radiology, University of Pennsylvania, Philadelphia, PA, United States

Background and Motivation: Analysis of long-bone cross-sectional images is essential for assessment of cortical bone structural properties [1]. Image analysis procedures such as quantification of anatomical geometry and imaging characteristic parameters require segmentation of the bone. We developed an automatic technique to segment the cortical and trabecular bone regions from cross-sectional MR images, from which geometric parameters can be computed such as cortical cross-sectional area and thickness and for overlaying parametric information such as bone water T1 and concentration. Analysis of these parameters allows monitoring changes longitudinally over time in the same subjects in response to treatment. This automatic software module reduces laborious manual segmentation and removes operator bias.

Methods: Anisotropic diffusion filtering [2] is applied as a preprocessing step to remove noise from the image while preserving the edges. The segmentation routine is initialized by the user selecting a location near the center of the marrow region. This initiates a region-growing algorithm with a threshold calculated dynamically by finding the standard deviation from the region-of-interest centered at the user's initialization point on the image. The marrow region is grown from the initialization point, terminating when the intensity difference between the adjacent voxel is greater than the threshold. In this manner the endosteal boundary enclosing the marrow region is detected (Fig 1a). The center of mass is then calculated from the resulting segmentation region mask and its center taken as the origin for polar transform (Fig 2a). Intensity profile along the radius with respect to each degree is drawn. The first-order derivative of each of these profiles is calculated (Fig 2b). The first and second positive peak of the derivative corresponds to the endosteal and periosteal boundary location, respectively, at each angular location. Inverse polar transform of these detected peaks then yields the complete periosteal boundary (Fig 1a). Segmentation mask can then be generated from these two boundaries to obtain geometric parameters (Fig 1b) and parametric images, for instance for computation of bone water T1 and concentration (Fig 1c).

Results and Conclusions: We tested the algorithm with images in subjects of different age, height and weight. The automatic segmentation results were in excellent agreement with those obtained by visually tracing polygons. From the 16 subjects in our data set, comparison between the parameters calculated from automatic and manual segmentation, the coefficient of determination (R^2) ranged from 0.84 to 0.96 and the slopes of the best-fit straight lines of all values from 0.93 to 1.09 over 6 consecutive slices. Results of individual parameters are presented in Table 1.

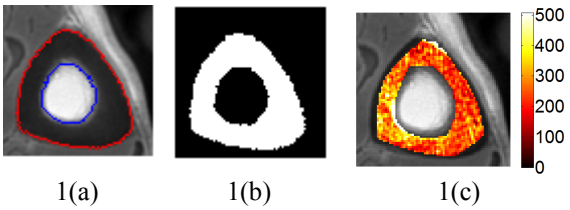

1(a) 1(b) 1(c)

Fig 1. (a) Periosteal (red) and endosteal boundary (blue) obtained by automatic segmentation; (b) Segmentation mask obtained from (a) for geometric parameter calculation; (c) T1 map (ms) calculated based on the mask (b) with 3 pixels of margin to remove the partial volume boundary effects.

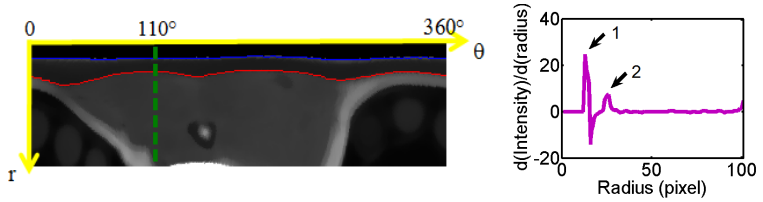

2(a) 2(b)

Fig 2. (a) Polar transform of Fig 1(a). Periosteal (red) and endosteal boundary (blue) obtained from the automatic segmentation algorithm. (b) Profile along radius (r) at θ=110°. Left (arrow 1) and right (arrow 2) positive peak corresponds to endosteal and periosteal boundary location detected at θ=110° respectively.

Table 1. Statistics of the differences in geometric and imaging parameters calculated from manual and automatic segmentation.

	Total bone area	Cortical bone area	Cortical thickness	Periosteal perimeter	Endosteal perimeter	T1
R^2	0.96	0.92	0.87	0.96	0.84	0.85
RMSD[#]	14.5 mm^2	14.8mm^2	0.34mm	1.6mm	2.1mm	11.9ms
Slope	0.99	1.09	0.98	0.98	1	0.93

RMSD[#]: Root mean squared difference

References: [1] Gomberg et al., Acad. Radiol. 2005; 12:1320-1332, [2] Perona and Malik, IEEE PAMI 1990; 12:629-639.

Acknowledgment: NIH RO1 50068